[2]Koide, S., Loria, A. F., and Babinsky, H., "Prediction of Shock Angles Caused by Sharp Delta Wings with Attack Angle," *AIAA Journal*, Vol. 36, No. 7, 1998, pp. 1327, 1328.

[3]Klunker, E. B., South, J. C., Jr., and Davis, R. M., "Calculation of Nonlinear Conical Flows by the Method of Lines," NASA TR R-374, Oct. 1971.

[4]Squire, L. C., "Pressure Distributions and Flow Patterns at $M = 4.0$ on some Delta Wings," British Aeronautical Research Council, Repts. and Memoranda, R&M 3373, London, Feb. 1964.

[5]Lu, F. K., Settles, G. S., and Horstman, C. C., "Mach Number Effects on Conical Surface Features of Swept Shock-Wave/Boundary-Layer Interactions," *AIAA Journal*, Vol. 28, No. 1, 1990, pp. 91–97.

[6]Rodi, P. E., and Dolling, D. S., "An Experimental/Computational Study of Sharp Fin Induced Shock Wave/Turbulent Boundary Layer Interactions at Mach 5: Experimental Results," AIAA Paper 92-0749, Jan. 1992.

[7]Settles, G. S., and Lu, F. K., "Conical Similarity of Shock/Boundary-Layer Interactions Generated by Swept and Unswept Fins," *AIAA Journal*, Vol. 23, No. 7, 1985, pp. 1021–1027.

[8]Deng, X. Y., and Liao, J. H., "Correlation of Conical Interactions Induced by Sharp Fins and Semicones," *AIAA Journal*, Vol. 31, No. 5, 1993, pp. 962, 963.

[9]Avduyevskiy, V. S., and Gretsov, V. K., "Investigation of a Three-Dimensional Separated Flow Around Semicones Placed on a Plane Plate," NASA TTF-13578, July 1971.

[10]Saida, N., Ooka, T., and Koide, S., "Interaction Between Shock Waves and Boundary Layer Induced by a Semicone Placed on a Flat Plate," *Journal of the Japan Society for Aeronautical and Space Sciences*, Vol. 33, No. 374, 1985, pp. 159–166 (in Japanese).

[11]Saida, N., Ogata, R., and Koide, S., "Shock Wave/Boundary Layer Interactions Induced by a Rhombic Delta Fin," *Journal of the Japan Society for Aeronautical and Space Sciences*, Vol. 48, No. 559, 2000, pp. 237–243 (in Japanese).

[12]Matsuo, K., "Shock Wave/Boundary Layer Interaction Induced by a Rhombic Delta Wing," M.S. Thesis, Dept. of Mechanical Engineering, Aoyama-Gakuin Univ., Setagaya, Tokyo, Jan. 2000 (in Japanese).

A. Plotkin
Associate Editor

Dynamics of an Orbiting Flexible Beam with a Moving Mass

D. C. D. Oguamanam* and J. S. Hansen†
University of Toronto, Toronto, Ontario M3H 5T6, Canada
and
G. R. Heppler‡
University of Waterloo, Waterloo, Ontario N2L 3G1, Canada

Introduction

THE operation of an early version of the International Space Station, in light of its large size and flexibility, gives reason to examine the effects that arise when the truss is traversed by the mobile servicing system. This has been partially investigated by Messac.[1,2]

Earth-based structures have been successfully modeled as elastic continua with traversing loads (or masses).[3–8] These studies highlight the influence of the magnitude of the traversing loads and the travel profile on the system dynamics. The dynamics of beams in general motion have been investigated by Ashley,[9] Sellappan and Bainum,[10] Kane et al.,[11] Meirovitch and Quinn,[12] Bainum and Li,[13] and Kirk and Lee.[14] The models in these studies can be looked upon as a satellite with an attached beam with a tip mass. The primary difference between these and the current study is that in the present work an additional mass is allowed to traverse the beam. The moving mass is modeled as a point mass, motion is restricted to the orbital plane, and the beam is modeled as an Euler–Bernoulli beam. Simulations are performed to examine the effect of various travel profiles on the system dynamics. Of particular interest are the elastic deformations under the moving mass and at the tip mass.

Received 29 December 2000; revision received 10 July 2001; accepted for publication 10 July 2001.

*Postdoctoral Fellow, Institute for Aerospace Studies, 4925 Dufferin Street.

†Professor, Institute for Aerospace Studies, 4925 Dufferin Street.

‡Professor, Systems Design Engineering. Senior Member AIAA.

Mathematical Formulation

The system under consideration is shown in Fig. 1; motion is restricted to the orbital plane. A satellite, modeled as a massive rigid body with center of mass located at $S^\star$ and with distance a from the center of mass to the base of the beam, is in a circular orbit of radius R_c about the Earth's center O. Because the satellite body is assumed to be much more massive than the other parts of the system, the appendage attached to the satellite is modeled as a beam cantilevered in the satellite fixed frame. The beam carries a point mass payload m_t at the tip of the beam, and it is traversed by a point mass m_v. The orbital frequency is ω_o, and the satellite spin rate is $\dot{\theta}$ about an axis perpendicular to the plane of the orbit.

The dynamics of the system are described by the aid of an inertial frame located at O with the dextral orthogonal basis $\mathcal{F}_e^T = [\boldsymbol{e}_1, \boldsymbol{e}_2, \boldsymbol{e}_3]$; an orbital frame with dextral basis $\mathcal{F}^T = [\boldsymbol{o}_1, \boldsymbol{o}_2, \boldsymbol{o}_3]$ is also located at O and is oriented such that the $\boldsymbol{o}_1$ is always passing through $S^\star$; a satellite body-fixed frame with dextral basis $[\boldsymbol{s}_1, \boldsymbol{s}_2, \boldsymbol{s}_3]$ is attached at $S^\star$.

The position vectors from O, to a spacecraft differential mass element $\boldsymbol{R}_s$, to an elemental mass of the beam $\boldsymbol{R}_b$, to the moving mass $\boldsymbol{R}_v$, and to the tip mass $\boldsymbol{R}_t$ are

$$\boldsymbol{R}_i = \boldsymbol{R}_c + \boldsymbol{r}_i, \qquad i \in \{b, s, t, v\} \tag{1}$$

The kinetic energy of the system $\mathcal{T}$ is

$$\mathcal{T} = \frac{1}{2}\int_{m_s} \dot{\boldsymbol{R}}_s \cdot \dot{\boldsymbol{R}}_s \,\mathrm{d}m_s + \frac{1}{2}\int_{m_b} \dot{\boldsymbol{R}}_b \cdot \dot{\boldsymbol{R}}_b \,\mathrm{d}m_b + \frac{1}{2}m_v\dot{\boldsymbol{R}}_v \cdot \dot{\boldsymbol{R}}_v + \frac{1}{2}m_t\dot{\boldsymbol{R}}_t \cdot \dot{\boldsymbol{R}}_t \tag{2}$$

where the first and second terms are caused by the satellite and the appendage, respectively. The penultimate term is the contribution of the moving mass, and the last term is caused by the tip mass. The velocities may be expanded as

$$\dot{\boldsymbol{R}}_b = \mathcal{F}_s^T \begin{bmatrix} R_c\omega_o \sin\theta - (\dot{\theta} + \omega_o)w(x,t) \\ 0 \\ R_c\omega_o\cos\theta + (\dot{\theta}+\omega_o)(a+x) + \dot{w}(x,t) \end{bmatrix} \tag{3}$$

$$\dot{\boldsymbol{R}}_v = \mathcal{F}_s^T \begin{bmatrix} \dot{x}_v + R_c\omega_o \sin\theta - (\dot{\theta} + \omega_o)w(x,t) \\ 0 \\ R_c\omega_o\cos\theta + (\dot{\theta}+\omega_o)(a+x) + \dot{w}(x,t) + \dot{x}_v \left.\dfrac{\partial w}{\partial x}\right|_{x=x_v} \end{bmatrix} \tag{4}$$

$$\dot{\boldsymbol{R}}_t = \dot{\boldsymbol{R}}_b(L_b, t) \tag{5}$$

where the angular velocity of the satellite with respect to the inertial frame is

$${}^E\boldsymbol{\omega}^s = -(\dot{\theta} + \omega_o)\boldsymbol{e}_2 \tag{6}$$

The time derivative of the deformation under the moving mass position $\mathrm{d}w/\mathrm{d}t$ introduces a convective term, which is a product of the moving mass speed and the slope of the deformation at the location of interest, as observed in Eq. (4).

The total potential energy is composed of the gravitational potential $\mathcal{U}_G$ and the strain energy $\mathcal{U}_S$:

$$\mathcal{U}_G = -\mu\left\{\int_{ms} |\boldsymbol{R}_s|^{-1}\,\mathrm{d}m_s + \int_{mb} |\boldsymbol{R}_s|^{-1}\,\mathrm{d}m_b + m_v|\boldsymbol{R}_v|^{-1} + m_t|\boldsymbol{R}_t|^{-1}\right\} \tag{7}$$

$$\mathcal{U}_S = \frac{1}{2}\int_0^{L_b} EI\left(\frac{\partial^2 w}{\partial x^2}\right)^2 \mathrm{d}x \tag{8}$$

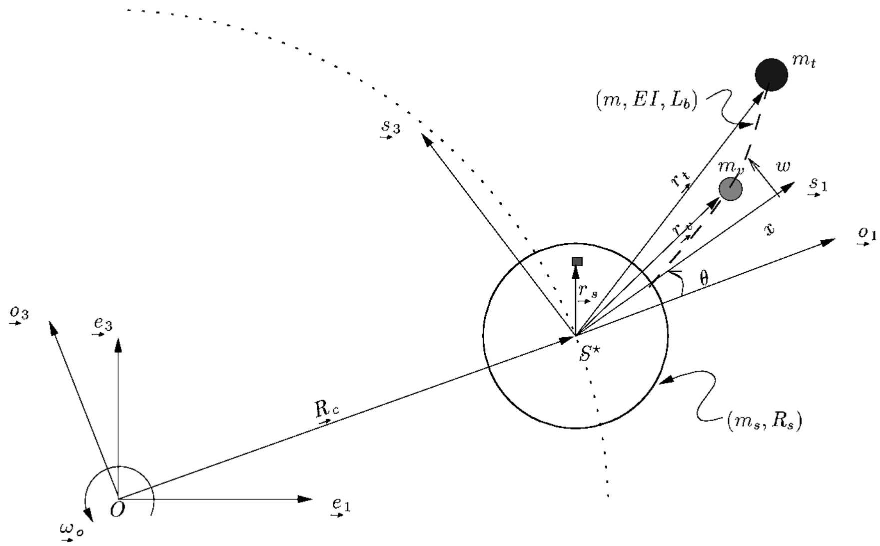

Fig. 1 Satellite-appendage-moving mass system.

where

$$|\boldsymbol{R}_i|^{-1} = R_c^{-1}\left\{1 - \frac{\boldsymbol{R}_c \cdot \boldsymbol{r}_i}{R_c^2} - \frac{\boldsymbol{r}_i \cdot \boldsymbol{r}_i}{2R_c^2} + \frac{3}{2R_c^4}(\boldsymbol{R}_c \cdot \boldsymbol{r}_i)^2\right\}$$

$$i \in \{b, s, t, v\}$$

It is advisable at this juncture to introduce the following nondimensional terms:

$$\xi \triangleq \frac{x}{L_b}, \qquad \xi_v \triangleq \frac{x_v}{L_b}, \qquad \eta \triangleq \frac{a}{L_b}$$

$$M_v \triangleq \frac{m_v}{\rho A L_b}, \qquad M_t \triangleq \frac{m_t}{\rho A L_b}, \qquad \lambda_i^4 \triangleq \frac{\rho A L_b^4 \omega_i^2}{EI} \tag{9}$$

The elastic deformation is assumed to be expressible in the separable form

$$w(x, t) = L_b \boldsymbol{W}^T(\xi)\boldsymbol{q}(t) \tag{10}$$

where $\boldsymbol{q}(t)$ is a column vector of undetermined coefficients and $\boldsymbol{W}(\xi)$ is a column vector of basis functions, which are the orthonormal eigenfunctions of a cantilever beam with tip mass. The following definitions are introduced for brevity:

$$\boldsymbol{M} \triangleq \int_0^1 \boldsymbol{W}\boldsymbol{W}^T \,\mathrm{d}\xi + M_t \boldsymbol{W}(1)\boldsymbol{W}(1)^T + M_v \boldsymbol{W}(\xi_v)\boldsymbol{W}(\xi_v)^T$$

$$\boldsymbol{K}_s \triangleq \frac{EI}{\rho A L_b^4}\int_0^1 \boldsymbol{W}''\boldsymbol{W}''^T \,\mathrm{d}\xi$$

$$\boldsymbol{F}_1 \triangleq \int_0^1 \boldsymbol{W} \,\mathrm{d}\xi + M_t \boldsymbol{W}(1) + M_v \boldsymbol{W}(\xi_v)$$

$$\boldsymbol{F}_2 \triangleq \int_0^1 \xi \boldsymbol{W} \,\mathrm{d}\xi + M_t \boldsymbol{W}(1) + M_v \xi_v \boldsymbol{W}(\xi_v) \tag{11}$$

Using Eq. (10) in Eqs. (2) and (7) and then forming the Lagrangian and following Hamilton's principle, the equations of motion, with reference to Eq. (11), are

$$\boldsymbol{M}\ddot{\boldsymbol{q}} + \boldsymbol{C}\dot{\boldsymbol{q}} + \boldsymbol{K}\boldsymbol{q} = \boldsymbol{F} \tag{12}$$

where

$$\boldsymbol{C} = 2M_v \dot{\xi}_v \boldsymbol{W}(\xi_v)\boldsymbol{W}'(\xi_v)^T$$

$$\boldsymbol{K} = \boldsymbol{K}_s + \left[\omega_o^2(1 - 3\sin^2\theta) - (\dot{\theta} + \omega_o)^2\right]\boldsymbol{M} + M_v\left[\dot{\xi}_v^2 \boldsymbol{W}(\xi_v)\boldsymbol{W}''(\xi_v)^T + \ddot{\xi}_v \boldsymbol{W}(\xi_v)\boldsymbol{W}'(\xi_v)^T\right]$$

$$\boldsymbol{F} = -\left[\ddot{\theta} + \tfrac{3}{2}\omega_o^2 \sin(2\theta)\right](\eta \boldsymbol{F}_1 + \boldsymbol{F}_2) - 2M_v \dot{\xi}_v(\dot{\theta} + \omega_o)\boldsymbol{W}(\xi_v) \tag{13}$$

The matrix $\boldsymbol{C}$ can be decomposed into a gyroscopic matrix $\boldsymbol{G}$ and a damping matrix $\boldsymbol{D}$ and $\boldsymbol{K}$ can be decomposed into a stiffness matrix $\hat{\boldsymbol{K}}$ and a circulatory matrix $\boldsymbol{H}$. In Eqs. (13) the orbital motion, the satellite spin, and the traversing mass motion all act as stiffness modulators in $\boldsymbol{K}$. These contributions will either soften or stiffen the beam depending on their signs, and the extent of the contribution will depend on their magnitude. The system is susceptible to instability because Eqs. (13) have the Hill–Mathieu form as a result of the harmonic stiffness modulators. The force vector $\boldsymbol{F}$ includes forces induced by the coupling of the traversing mass motion with the orbital motion and with the satellite spin motion. The remaining components of the forcing term are the forces induced by the orbital motion and by the satellite spin motion.

In the simulations it is important to retain the nonlinear contribution of the traverse speed because the beam deflections obtained from a linear analysis are usually smaller than those obtained with the nonlinear analysis for sufficiently large traversal speeds.[4,6] A modified Newmark scheme[8] is implemented because of the time dependency of $\boldsymbol{M}$, $\boldsymbol{C}$, $\boldsymbol{K}$, and $\boldsymbol{F}$.

Simulation and Discussion

The material properties of the simulated beam are from Kirk and Lee,[14] except that $L_b = 60$ m. Three phases define the travel profile of the moving mass. The phases are demarcated by the times $[0, t_1, t_2, t_f]$; the first phase is defined by a quintic polynomial that prescribes an acceleration from rest to a constant velocity in time t_1. The attained velocity is held constant during the second phase from $t_1 - t_2$, and in the third phase the quintic polynomial prescribes a deceleration to rest at t_f. The simulations are based on an assumed 6000-s orbit period and a spin period of 600 s. Three traversal profiles are examined: all have $t_f = 60$ s with, for profile A, $(t_1, t_2) = (10, 50)$; for profile B, $(t_1, t_2) = (15, 45)$; and for profile C, $(t_1, t_2) = (20, 40)$. These profiles are in ascending (descending) order of maximum attained velocity (acceleration). The nondimensional traversing and tip masses are $M_v = 0.15$ and $M_t = 0.10$, respectively. All of the results were obtained by using a Rayleigh–Ritz formulation that employed the first five modes of the structure. These modes had the frequencies 0.5592, 3.767, 10.95, 22.01, and 37.00 Hz. Figure 2 depicts the deformation of the beam under the moving mass for the various traversal profiles. The beam deflection under the moving mass when $t \le 10$ s does not show any significant differences between the traversal profiles. The differences are more pronounced on $10 \le t \le 20$, and it can be observed that the magnitude of the deformations occurs in decreasing order for profiles A, B, and C. In this segment traversal profile C exhibits the maximum velocity and acceleration, followed, in order, by profiles B and A. With reference to Eqs. (13), the higher velocity would contribute higher forcing and also larger stiffness modulation. The higher

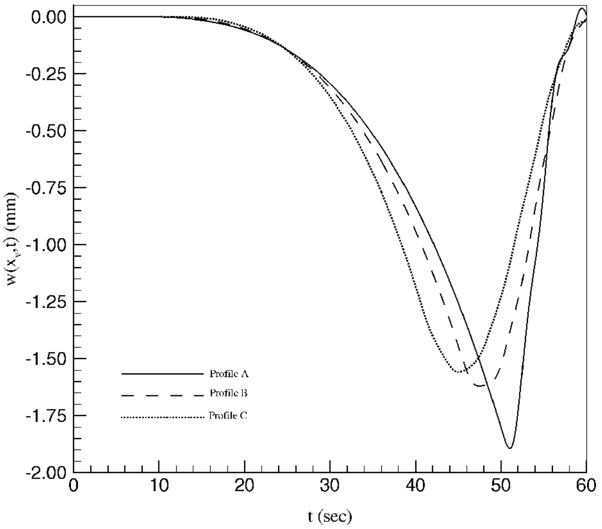

Fig. 2 Deflection under moving mass for various travel profiles.

acceleration contributes to a larger stiffness modulation. Given that profile A displayed the maximum deformation but the least velocity and acceleration, it is probable that, in this example, the role played by velocity in the forcing term dominates the combined stiffening effects of velocity and acceleration.

At a point that is within the constant velocity phase, these three curves cross one another so that now C exhibits the greatest deflection, followed by B, and then A. The deformations in the constant velocity phase indicate that the forcing terms dominate over the stiffening components. The magnitude of the deformations across the profiles is proportional to the magnitude of the constant velocity attained during this phase. The continued increasing deformation exhibited by profiles B and C is a consequence of their longer constant velocity phase during which energy is further added to the system.

The magnitude of the velocity forcing term decreases over the third phase, and the deceleration softens the stiffness modulation. This explains the decreasing deformation experienced with each traversal profile. Hence the reversal in the magnitudes of the deformation such that, during approximately the last 10 s, profile A deforms the most, followed by B, and then C. The deformation of profile B is bounded by the profiles A and C because the velocities and accelerations of the traversing mass are similarly bounded.

Based on the examined profiles, it can be inferred that, using the relative magnitude of the deformation under the traversing mass as a basis for comparison, the travel profile with the minimum constant velocity phase duration is the best choice. Although the profile with the minimum constant velocity phase duration has the maximum constant velocity and hence experiences the greatest forcing, it receives the smallest impulse. The traversing mass acceleration is not modulating the stiffness of the system during this phase because it is zero. The same profile has the least deceleration, which corresponds to the least softening effect, which in turn implies the least deformation.

Conclusions

The system of governing equations for the planar orbiting dynamics of a flexible beam attached to a satellite and traversed by a moving mass show that the velocity and acceleration of the traversing mass act as stiffness modulators. The former appears in a quadratic form and was retained during the simulations because the velocity at which its contribution is negligible is not intuitively evident. The velocity of the traversing mass also contributes to the system forcing term. It is inferred from the simulated travel profiles that it is best, based on the relative magnitudes of the system deformations, to use a travel profile with the shortest constant velocity phase, or equivalently the smallest possible accelerations and decelerations.

References

[1]Messac, A., "Flexible-Body Dynamics Modeling of a Vehicle Moving on Rails of a Structure," *Journal of Guidance, Control, and Dynamics*, Vol. 19, No. 3, 1996, pp. 540–548.

[2]Messac, A., "Dynamics Modeling of a Flexible Vehicle Moving on the Rails of a Flexible Structure," AIAA Paper 94-1614, April 1994.

[3]Frýba, L., *Vibrations of Solids and Structures Under Moving Loads*, Noordhoff International, Leyden, The Netherlands, 1972.

[4]Oguamanam, D. C. D., Hansen, J. S., and Heppler, G. R., "Dynamics of a Three-Dimensional Overhead Crane System," *Journal of Sound and Vibration*, Vol. 242, No. 3, 2001, pp. 411–426.

[5]Siddiqui, S. A. Q., Golnaraghi, M. F., and Heppler, G. R., "Dynamics of a Flexible Beam Carrying a Moving Mass Using Perturation, Numerical and Time-Frequency Analysis Techniques," *Journal of Sound and Vibration*, Vol. 229, No. 5, 2000, pp. 1023–1055.

[6]Sadiku, S., and Leipholz, H. H. E., "On the Dynamics of Elastic Systems with Moving Masses," *Ingenieur-Archiv*, Vol. 57, No. 3, 1987, pp. 223–242.

[7]Stanišić, M. M., "On a New Theory of the Dynamic Behaviour of Structures Carrying Moving Masses," *Ingenieur-Archiv*, Vol. 55, No. 3, 1985, pp. 176–185.

[8]Olsson, M., "Finite Element, Modal Co-Ordinate Analysis of Structures Subjected to Moving Loads," *Journal of Sound and Vibration*, Vol. 99, No. 1, 1985, pp. 1–12.

[9]Ashley, H., "Observations on the Dynamic Behavior of Large Flexible Bodies in Orbit," *AIAA Journal*, Vol. 5, No. 3, 1967, pp. 460–469.

[10]Sellappan, R., and Bainum, P. M., "Modal Control of the Planar Motion of a Long Flexible Beam in Orbit," *Acta Astronautica*, Vol. 7, No. 1, 1980, pp. 19–36.

[11]Kane, T. R., Ryan, R. R., and Banerjee, A. K., "Dynamics of a Cantilever Beam Attached to a Moving Base," *Journal of Guidance, Control, and Dynamics*, Vol. 10, No. 2, 1987, pp. 139–151.

[12]Meirovitch, L., and Quinn, R. D., "Equations of Motion for Maneuvering Flexible Spacecraft," *Journal of Guidance, Control, and Dynamics*, Vol. 10, No. 5, 1987, pp. 453–465.

[13]Bainum, P. M., and Li, F., "Optimal Large Angle Maneuvers of a Flexible Spacecraft," *Acta Astronautica*, Vol. 25, No. 3, 1991, pp. 141–148.

[14]Kirk, C. L., and Lee, M. S., "Proof-Mass Actuator Control of Shuttle-Based Astromast," *Acta Astronautica*, Vol. 32, No. 2, 1994, pp. 97–106.

A. Messac
Associate Editor

Cyclic Creep of Piezoelectric Polymer Polyvinylidene Fluoride

A. M. Vinogradov* and S. C. Schumacher†
Montana State University, Bozeman, Montana 59717

Nomenclature

t	=	time
ε_m	=	creep strain
ε_v	=	vibrocreep strain
σ_a	=	stress amplitude
σ_m	=	mean stress
ω	=	frequency

Introduction

IN the past few decades a new generation of synthetic piezoelectric polymers has emerged that possess the ability to actively react to changing stimuli as a result of energy conversion from mechanical to electrical and vice versa. Piezoelectric polymer systems have been increasingly integrated in structural design as active elements capable of sensing and responding intelligently to external stimuli. A broad range of applications utilizing such functions include active vibration damping, acoustic suppression, damage detection, shape and position control of compliant structures, and self-inspection of structural integrity.[1,2]

Received 19 February 2001; presented as Paper 2001-1413 at the AIAA/ASME/ASCE/AHS/ASC 42nd Structures, Structural Dynamics, and Materials Conference, Seattle, WA, 16–19 April 2001; revision received 5 July 2001; accepted for publication 10 July 2001.

*Professor, Department of Mechanical and Industrial Engineering, 220 Roberts Hall. Member AIAA.

†Graduate Student, Department of Mechanical and Industrial Engineering, 220 Roberts Hall.